npj | 2D Materials and Applications

www.nature.com/npj2dmaterials

ARTICLE OPEN

Substrate engineering of graphene reactivity: towards high-performance graphene-based catalysts

Na Guo[1], Kah Meng Yam[1,2] and Chun Zhang[1,2]

Graphene-based solid-state catalysis is an emerging direction in research on graphene, which opens new opportunities in graphene applications and thus has attracted enormous interests recently. A central issue in graphene-based catalysis is the lack of an effective yet practical way to activate the chemically inert graphene, which is largely due to the difficulties in the direct treatment of graphene (such as doping transition metal elements and introducing particular type of vacancies). Here we report a way to overcome these difficulties by promoting the reactivity and catalytic activity of graphene via substrate engineering. With thorough first-principles investigations, we demonstrate that when introduce a defect, either a substitutional impurity atom (e.g. Au, Cu, Ag, Zn) or a single vacancy, in the underlying Ru (0001) substrate, the reactivity of the supported graphene can be greatly enhanced, resulting in the chemical adsorption of O_2 molecules on graphene. The origin of the O_2 chemical adsorption is found to be the impurity- or vacancy-induced significant charge transfer from the graphene–Ru (0001) contact region to the $2\pi^*$ orbital of the O_2 molecule. We then further show that the charge transfer also leads to high catalytic activity of graphene for chemical reaction of CO oxidation. According to our calculations, the catalyzed CO oxidation takes place in Eley-Rideal (ER) mechanism with low reaction barriers (around 0.5 eV), suggesting that the substrate engineering is an effective way to turn the supported graphene into an excellent catalyst that has potential for large-scale industrial applications.

npj 2D Materials and Applications (2018)2:1 ; doi:10.1038/s41699-017-0046-y

INTRODUCTION

Recent research effort has shown that graphene has potential applications not only in solid-state physics as a promising electronic material[1] but also in solid-state chemistry as a novel catalyst or support of catalysts.[2–11] Since graphene itself is chemically inert, a central issue in designing graphene-based solid-state catalysts (GBSSCs) is to promote reactivity and catalytic activity of graphene in an efficient yet practical way. In literature, various methods for activating graphene such as applying a mechanical strain[3], introducing vacancy defects[4], impurity doping[5–8], and decorating graphene with functional groups[9,10] have been proposed. Some unusual and exciting features of GBSSCs have been reported, making graphene a seemingly promising candidate for solid-state catalysts. However, all these previously suggested GBSSCs require direct treatments of graphene[3–10] and/or specially designed ultra-thin metal layer[8], which are very difficult (if not impossible) to realize in a controllable manner in experiments, therefore present great challenges for large-scale production in industry. The lack of efficient and easy-to-control way of activating graphene has now become the major factor that limits the future development of GBSSCs. Here with comprehensive computational modeling, we describe an interesting way to greatly promote reactivity and catalytic activity of graphene via engineering the underlying substrate with defects. Defects include substitution impurity atoms and also vacancies. Compared with previous suggestions, the substrate engineering proposed here is much more practical and easier to control since no ultra-thin metal layer between substrate and graphene is needed and the direct treatment of graphene is avoided. We expect our findings to stimulate new experiments, and pave the way for future design of GBSSCs that are good for large-scale industrial applications.

A schematic illustration of the substrate engineering for reactivity of graphene is given in Fig. 1, where graphene is supported on a substrate that is engineered with defects, a substitutional impurity atom (IA) and a vacancy (V). The defect (IA or V) changes the interaction between graphene and the substrate, resulting in possibly different local chemical properties of those graphene parts right above the defect (areas enclosed by red dotted circles in the figure). We expect that by appropriately choosing types of IA and V, the reactivity of those local parts can be greatly enhanced. In this paper, the substrate is chosen to be Ru (0001) that has been widely used as graphene support[12–14] and the reactivity of graphene is tested by O_2 adsorption. As demonstrated in the figure, O_2 molecules chemically bind onto the activated parts of graphene, while other parts of graphene remain inactive for O_2 adsorption.

RESULTS AND DISCUSSIONS

Graphene supported on Ru (0001)

It has been shown that the epitaxial high-quality monolayer graphene with macroscale size can continuously form on Ru (0001),[12–14] which makes Ru (0001) one of the most promising substrates for graphene applications. Density functional theory

[1]Department of Physics and Centre for Advanced 2D Materials, National University of Singapore, Singapore 117551, Singapore and [2]Department of Chemistry, National University of Singapore, Singapore 117542, Singapore
Correspondence: Chun Zhang (phyzc@nus.edu.sg)
Na Guo and Kah Meng Yam contributed equally to this work.

Received: 17 August 2017 Revised: 28 December 2017 Accepted: 29 December 2017
Published online: 17 January 2018

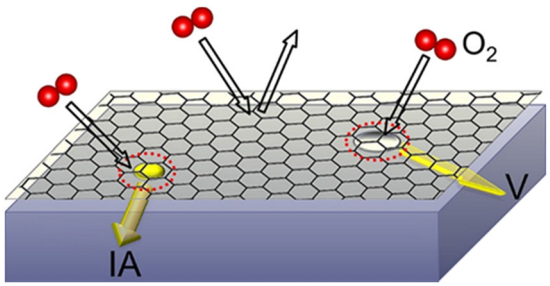

Fig. 1 Schematic illustration of substrate engineering for reactivity of graphene. When the underlying substrate has a defect (either a substitutional impurity atom (IA) or a vacancy (V)), the local chemical properties of supported graphene right on top of IA or V (the parts enclosed by red dotted circles) may be affected so that O_2 molecules can be chemically adsorbed. Other parts of graphene remain inactive for O_2 adsorption

(DFT)-based computational modeling is the commonly used theoretical tool to understand physical and chemical properties of Ru (0001)-supported graphene.[15–17] In literature, two different types of DFT-based approaches have been used. The first one uses a very large supercell (e.g., 11×11 graphene unit cells)[17] to describe the so-called moiré pattern originated from the lattice mismatch between graphene and Ru. This approach is able to produce the long-range variation of the lattice that agrees well with experiments, but extremely expensive so that is not applicable for some detailed analysis such as chemical reactivity and catalytic activity of the supported graphene. The second approach (which is more often used) employs a much smaller supercell with stretched lattice constant of graphene (to match the Ru (0001) lattice).[15–17] Previous studies have convincingly shown that although the second approach (the stretched model) neglects the long-range lattice variation (the moiré pattern), it does generate essentially the same electronic properties of the system as those obtained from the first approach, therefore can correctly describe the interaction between graphene and Ru (0001) and are good for further analysis.

In this paper, we adopt the second approach in our computational studies. In particular, we use a supercell that contains 4×4 graphene cells and the graphene cell is stretched to match the lattice of Ru (0001). Following the common practice in previous DFT calculations, we consider here three possible different adsorption configurations of graphene@Ru (0001): fcc-top, hcp-top, fcc-hcp (as shown in Fig. 2a–c, respectively). An additional configuration (the intermediate one between fcc-top and hcp-top as shown in Fig. 2d) is also found to be stable in our calculations. For the fcc-hcp case, there is no chemical binding between graphene and Ru (0001), and, for both fcc-top and and hcp-top configurations, the adsorption energy of graphene is estimated to be around −0.4 eV per C with the distance between graphene and Ru surface (d_{G-Ru}) around 2.16 Å, all of which agree well with previous calculations. For the intermediate configuration, our calculations yield the graphene adsorption energy about −0.3 eV/C and d_{G-Ru} around 2.10 Å. The isosurfaces of charge redistribution clearly indicate that chemical bonds form between graphene and Ru surface for fcc-top, hcp-top, and intermediate cases. Note that here the charge redistribution is defined as the electron density difference between graphene@Ru (0001) and the two separated systems: $\delta\rho = \rho_{G@Ru} - (\rho_G + \rho_{Ru})$. Further calculations for all of these four configurations show that when supported on Ru (0001), graphene is still inactive so that O_2 molecules do not chemically bind on it. Next we will try to activate graphene via the aforementioned substrate engineering.

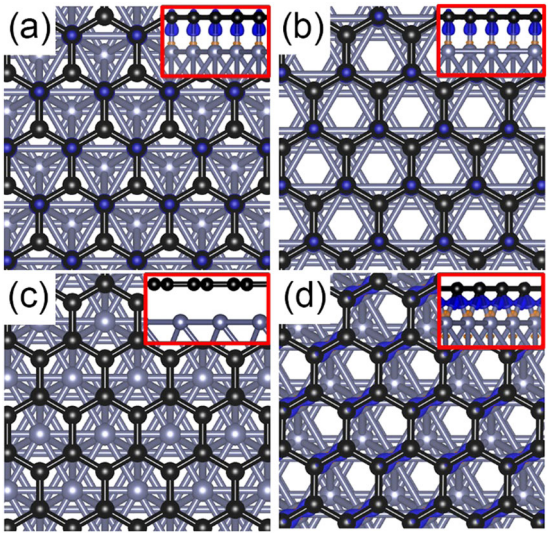

Fig. 2 Four possible adsorption configurations of graphene@Ru (0001): **a** fcc-top, **b** hcp-top, **c** fcc-hcp, and **d** intermediate. Color Scheme: Carbon in black and Ru in gray. Isosurface of charge redistribution is also shown: Blue (brown) represents electron accumulation (depletion). Insets: Side views of adsorption configurations. The charge redistribution is defined as $\delta\rho = \rho_{G@Ru} - (\rho_G + \rho_{Ru})$. Note that there is no visible charge redistribution in **c**, indicating the weak interaction between graphene and Ru surface in this case

Engineering the Ru (0001) substrate with substitutional impurity atoms

The major idea of this paper is to tune the reactivity of graphene by engineering the underlying substrate with defects, which enables us to avoid the direct treatment of graphene. Two types of defects (IA and V as aforementioned) are to be tested. In this section, we investigate the effects of IA on reactivity and catalytic activity of the supported graphene. Four different types of impurities, Au, Ag, Cu, and Zn, are studied. We show that all these impurities in the substrate are able to dramatically promote the reactivity and also the catalytic activity of the supported graphene, leading to chemical adsorption of O_2 molecules and low reaction barriers of CO oxidation. In Fig. 3, we plot the optimized atomic structures of graphene supported on Ru (0001) with an Au impurity. All four possible adsorption configurations as mentioned earlier are considered. The charge redistribution caused by the Au impurity defined as $\delta\rho = \rho_{G@doped\,Ru} - \rho_{G@Ru}$ is also shown in the figure. Other impurity cases are shown in the supplemental material (Figures S1–S3).

From Fig. 3, we can see that with the Au impurity in Ru (0001), the supported graphene still remains flat, while, for fcc-top, hcp-top, and intermediate cases, the impurity causes the charge transfer from the graphene–Ru contact region to the impurity and also C atoms right on top of it. The impurity-atom induced electron accumulation can also be verified by the electron localized function (ELF) as shown in the upper panel of Figure S4 (supplemental material). Such charge transfer weakens the chemical bonds between these affected C atoms and the substrate, resulting in a weaker graphene adsorption (increase in adsorption energy around +0.06 eV per C) compared with undoped cases for all these three configurations. For the fcc-hcp case (Fig. 3c), as expected, the Au impurity has negligible effects on graphene for the fcc-hcp configuration due to the weak interaction between graphene and Ru surface in this case.

We expect the Au-impurity-induced charge transfer (Fig. 3a, b, d) to create a local region in the supported graphene with different chemical properties from other parts. Our calculations

indeed show that the reactivity of these local regions in graphene is greatly enhanced compared with other parts. As a result, O_2 molecule chemically binds onto these local regions with significant adsorption energies, −0.43 eV for fcc-top, −0.72 eV for hcp-top, and −0.53 eV for intermediate case (there is no O_2 chemical adsorption for the fcc-hcp case). The O_2 adsorption configurations are shown in Fig. 4. The isosurfaces of charge redistribution caused by the O_2 adsorption is also superimposed in the figure. The charge transfer from the graphene to O_2 2π* orbital can be clearly seen. To further illustrate the charge transfer, we plot in Fig. 4d the density of states (DOS) of O_2 *p* orbital before and after adsorption for the fcc-top case. Before adsorption, O_2 is magnetic with an empty spin-down 2π* orbital. After adsorption, electrons transfer to the empty 2π* orbital, pulling it down to be below Fermi energy and eliminating the magnetism. The charge transfer also leads to the significant elongation of O–O bond of the adsorbed O_2 molecule. In Table 1, we list the O_2 adsorption energies, charge transfer, and O–O bond lengths for fcc-top, hcp-top, and intermediate configurations. Note that O_2 does not bind on graphene for the fcc-hcp case. Other impurities (e.g. Ag, Cu, and Zn) can also promote the reactivity of the supported graphene, leading to O_2 chemical adsorptions (see Figures S5–S7 and Table S1 in the supplemental material). The impurity induced significant elongation of O–O bond (from its gas-phase value 1.23 Å) implies the activation of the O_2 molecule. We next probe the catalytic activity of the supported graphene using the catalyzed chemical reaction of CO oxidation.

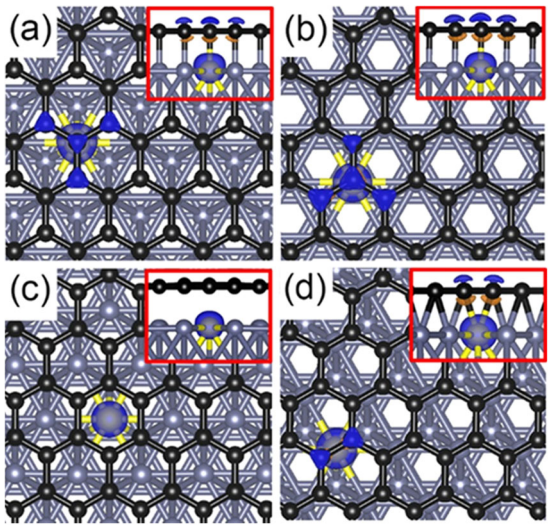

Fig. 3 Graphene@Ru (0001) with an Au impurity (in yellow). **a** fcc-top, **b** hcp-top, **c** fcc-hcp, and **d** intermediate. Charge redistribution caused by the Au impurity is also shown. Color scheme is the same as in Fig. 2. The Au impurity has no visible effects on the supported graphene for the fcc-hcp case

In most cases, a complete cycle of the catalyzed CO oxidation consists of two steps: (1) one CO is oxidized by one O, $CO + O_2 \Rightarrow CO_2 + O^*$; (2) another CO comes and brings away the leftover O atom, $CO + O^* \Rightarrow CO_2$. Since the CO molecule does not bind onto the supported graphene, the catalyzed reaction happens in Eley-Rideal (ER) mechanism. With the cNEB method, we investigate the ER type of CO oxidation catalyzed by graphene@Ru (0001) with Au for fcc-top, hcp-top, and intermediate configurations (The fcc-hcp configuration is not catalytically active). The energy profile along the reaction path for the fcc-top case is shown in Fig. 4e, f. Both the two steps of the CO oxidation have low reaction barriers around 0.5 eV. Other two configurations, hcp-top and intermediate, generate similar low barriers with the highest value around 0.6 eV (see Table 2 and also Figures S8 and S9 in the supplemental material), clearly suggesting that the graphene supported on Ru (0001) with an Au impurity is an excellent catalyst for CO oxidation. Similar to Au, other impurities we tested, Ag, Cu, and Zn, also lead to high catalytic activity of the supported graphene (see Figures S10–S18 and Table S2 in the supplemental material). According to our calculations, the best catalytic performance occurs for the Ag impurity in the intermediate configuration, which gives the reaction barriers less than 0.4 eV for both reaction steps (Table S2).

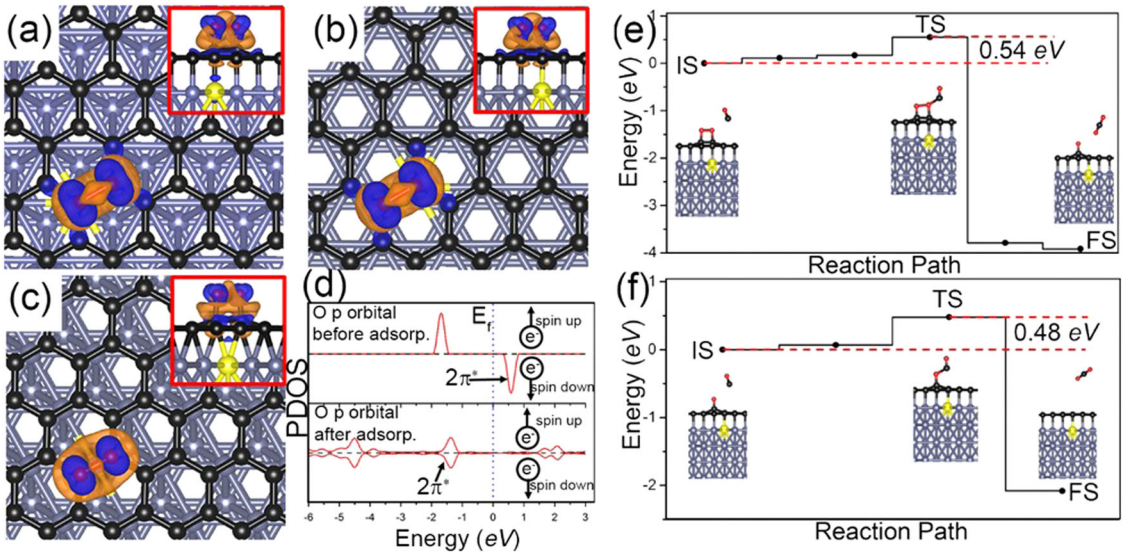

Fig. 4 O_2 (in red) adsorption on graphene@Ru (0001) with an Au impurity: **a** fcc-top, **b** hcp-top, and **c** intermediate. Isosurfaces of the charge redistribution caused by O_2 adsorption is superimposed. The charge redistribution is defined as $\delta\rho = \rho_{O_2@G@Ru} - (\rho_{G@Ru} + \rho_{O_2})$. Note that O_2 does not bind onto graphene for the fcc-hcp case. Partial density of states of O_2 *p* orbital before/after adsorption for fcc-top configuration is shown in **d**. The upper (lower) panel in **d** is for the case of before (after) adsorption. Energy profile along the reaction path for two steps of CO oxidation catalyzed by fcc-top Graphene@Ru (0001) with Au in ER mechanism: **e** $CO + O_2 \Rightarrow CO_2 + O^*$ and (**f**) $CO + O^* \Rightarrow CO_2$. Atomic structures of the initial state (IS), the transition state (TS), and the final state (FS) are also shown. Calculations are done with cNEB method.Color scheme is the same as before

Table 1. O_2 adsorption on graphene@Ru (0001) with Au

Configuration	E_{ad} (*eV*)	ΔQ (e^-)	O–O (Å)
fcc-top	−0.43	0.99	1.48
hcp-top	−0.72	0.98	1.48
Intermediate	−0.52	1.03	1.48

E_{ad} adsorption energy of O_2, ΔQ electrons transferred to O_2, O–O O–O bond length of O_2

Table 2. Reaction barriers of the CO oxidation catalyzed by graphene@Ru (0001) with Au in hcp-top and intermediate configurations

Configuration	E_b^{1st} (eV)	E_b^{2nd} (eV)
hcp-top	0.61	0.57
Intermediate	0.62	0.45

E_b^{1st} and E_b^{2nd} are barriers of the first and second step of CO oxidation respectively

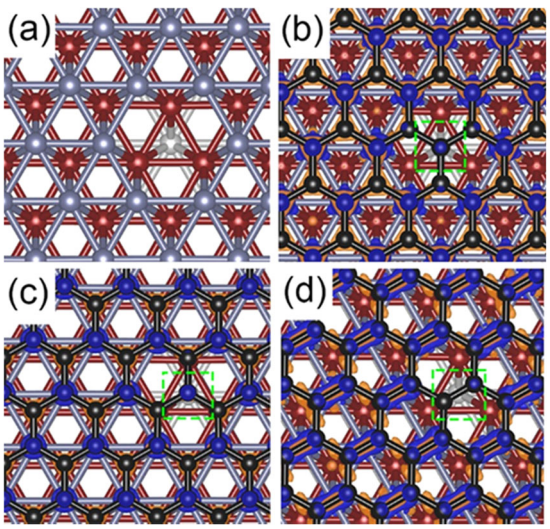

Fig. 5 **a** The optimized atomic model of Ru (0001) surface with a single vacancy: The first top layer in gray, second layer in dark red, and the third layer in silver. The vacancy is on the first layer. The **b** fcc-top, **c** hcp-top, and **d** intermediate adsorption configuration of graphene on Ru (0001) with a single vacancy. Isosurfaces of charge redistribution caused by the graphene adsorption is superimposed in **b**–**d**: Blue (brown) represents accumulation (depletion) of electrons. C atoms right above the vacancy are enclosed by green dashed squares. The charge redistribution is defined as the electron density difference induced by the graphene adsorption, $\delta\rho = \rho_{G@Ru} - (\rho_G + \rho_{Ru})$

Engineering the Ru (0001) substrate with vacancy

Another way to engineer the properties of substrate is to introduce vacancies. As a demonstration, here we consider the simplest case, a single vacancy in Ru (0001). We will show that similar to the impurity case, a vacancy in the substrate can also greatly promote the reactivity and catalytic activity of the supported graphene.

In Fig. 5a, we show the optimized atomic model of Ru substrate with a single vacancy on its (0001) surface. In order to see the vacancy more clearly, we plot the different Ru layers in different colors. The fcc-top, hcp-top, and the intermediate graphene adsorption configurations are shown in Fig. 5b–d, respectively. The fcc-hcp case is neglected here since we have known from the previous section that the substrate has negligible effects on the supported graphene in this case. The charge redistribution caused by graphene adsorption, defined as $\delta\rho = \rho_{G@Ru} - (\rho_G + \rho_{Ru})$, is also shown in the figure, from which we can see that similar to impurity cases, C atoms right above the vacancy (those enclosed in a green dashed squares) are chemically 'different' from other parts of graphene due to the weak bonding between these atoms and Ru substrate. ELF calculations show that with a vacancy, electrons also tend to accumulate on these C atoms (see Figure S4 in supplemental material). We therefore expect that these C atoms can be more reactive than others. Indeed, our calculations show that O_2 molecules chemically bind onto these C atoms with significant adsorption energies, −0.29 eV for fcc-top, −0.49 eV for hcp-top, and −0.58 eV for intermediate case. In contrast, other parts of graphene still remain inert so that there is no chemical adsorption of O_2 molecules. The O_2 adsorption configurations for different cases are shown in Fig. 6 with isosurfaces of O_2 induced charge redistribution superimposed. Similar to impurity cases, there are significant charge transfer to O_2 2π* orbital for all cases, which can be more clearly seen from partial DOS of *p* orbital of O_2 (Fig. 6d). The amount of charge transfer and also the significantly elongated O–O bond length for all cases are summarized in Table 3.

We now study the effects of the vacancy in the underlying substrate on catalytic activity of the supported graphene by calculating reaction barriers of the catalyzed CO oxidation using the cNEB method. The energy profile along the reaction path for the fcc-top case is shown in Fig. 6e, f. The reaction takes place in ER mechanism due to the fact that CO molecules do not bind onto graphene for all cases. The first step of the reaction (Fig. 6e) has a very low reaction barrier (0.32 eV), and the barrier for the second step CO oxidation (Fig. 6f) is around 0.53 eV, indicating the vacancy induced high catalytic activity of the supported graphene. Energy profiles for the reaction catalyzed by other two configurations (hcp-top and intermediate one) can be found in Figures S19 and S20 in the supplemental material. The calculated reaction barriers of these two cases are summarized in Table 4. All these results indicate that the vacancy in the substrate can be an effective way to greatly promote the catalytic activity of the supported graphene.

CONCLUSIONS

In summary, via intensive first-principles calculations, we demonstrate an intriguing way to drastically promote reactivity and catalytic activity of graphene via engineering the underlying substrate with defects. We show that when a defect, either a substitutional IA or a single vacancy, is introduced into the underlying substrate (Ru (0001) in this paper), the reactivity of the supported graphene can be greatly enhanced. As a result, O_2 molecules can be chemically adsorbed on graphene right above the defect in the substrate. The origin of the O_2 chemical adsorption is found to be the impurity- or vacancy-induced significant charge transfer from the graphene–Ru (0001) contact region to the 2π* orbital of the O_2 molecule. We then further show that the charge transfer also leads to high catalytic activity of graphene for chemical reaction of CO oxidation. According to our calculations, the catalyzed CO oxidation takes place in ER mechanism with low reaction barriers (around 0.5 eV). Together with reasonable formation energies of those impurities and vacancy we considered (Table S3 in supplemental material), our studies show that the substrate engineering can be a very practical and efficient way to turn the supported graphene into an excellent catalyst. Our calculations also suggest that two factors are important in the defect-in-substrate enhanced reactivity and catalytic activity of graphene: The strong chemical interaction

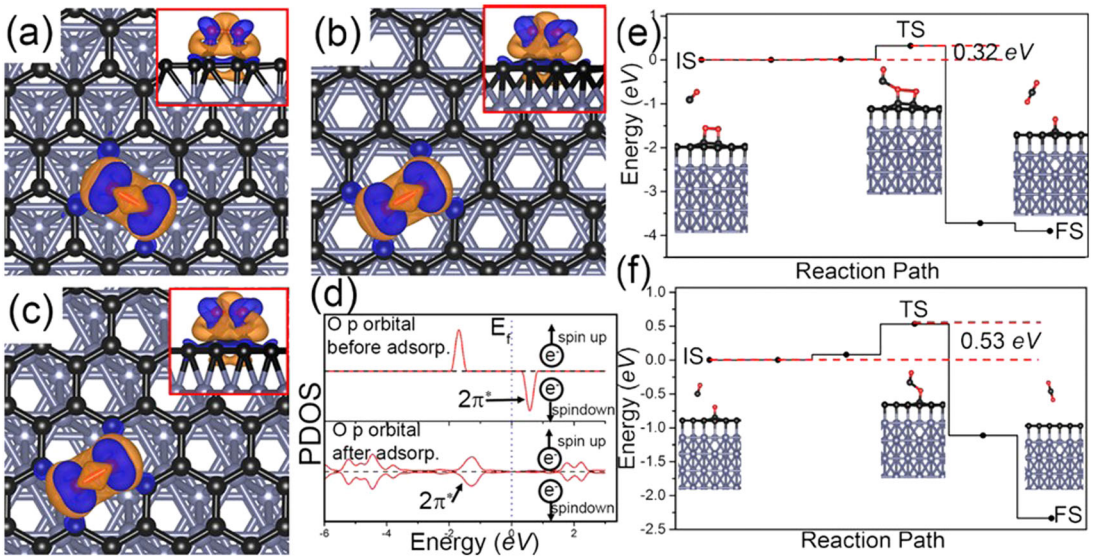

Fig. 6 O_2 adsorption on graphene@Ru (0001) with a single vacancy: **a** fcc-top, **b** hcp-top, and **c** intermediate. Isosurfaces of the charge redistribution caused by O_2 adsorption is superimposed. The charge redistribution is defined as $\delta\rho = \rho_{O_2@G@Ru} - (\rho_{G@Ru} + \rho_{O_2})$. Partial density of states of O_2 *p* orbital before/after adsorption for fcc-top configuration is shown in **d**. The upper (lower) panel in **d** is for the case of before (after) adsorption. cNEB calculations for two reaction steps of CO oxidation catalyzed by fcc-top Graphene@v-Ru(0001) in ER mechanism: **e** $CO + O_2 \Rightarrow CO_2 + O^*$ and **f** $CO + O^* \Rightarrow CO_2$

Table 3. O_2 adsorption on graphene@Ru (0001) with a single vacancy

Configuration	E_{ad} (eV)	ΔQ (e^-)	O–O (Å)
fcc-top	−0.29	1.02	1.48
hcp-top	−0.49	1.02	1.48
Intermediate	−0.58	0.98	1.48

Table 4. Reaction barriers of the CO oxidation catalyzed by graphene@Ru (0001) with a single vacancy in hcp-top and intermediate configurations

Configuration	E_b^{1st} (eV)	E_b^{2nd} (eV)
hcp-top	0.25	0.51
Intermediate	0.65	0.87

between the defect-free substrate and the supported graphene, and the defect-induced significant weakening of the interaction. These results provide guidelines for the design of a new family of high-performance graphene-based solid-state catalysts that may have potential for large-scale industrial applications.

COMPUTATIONAL METHODS

The first-principles calculations are performed with spin-polarized DFT as implemented in Vienna ab-initio Simulation Package (VASP).[18,19] van der Waals (vdW) interactions are considered through the so-called DFT+D2 method.[20] Activation barriers of catalyzed chemical reactions (CO oxidation in this paper) are determined by the Climbing Image Nudged Elastic Band (cNEB) method.[21] The generalized gradient approximation in the Perdew-Burke-Ernzerhof format[22] and the projector augmented wave method[23] are employed in all calculations. A plane wave basis with the cut-off energy of 400 eV is used. The convergence criterion for structural relaxations is set to 0.01 eV/Å.

Data availability

The datasets generated during and/or analyzed during the current study are available from the corresponding author on reasonable request.

ACKNOWLEDGEMENTS

We acknowledge the support from Singapore National Research Foundation (NRF-CRP13-2014-03 and NRF-CRP16-2015-02), Singapore Ministry of Education (R143-000-A06-112), and NUS academic research grants (R144-000-344-112). Computations were performed at the Graphene Research Centre at NUS.

AUTHOR CONTRIBUTIONS

C.Z. designed and supervised the project. N.G. and K.M.Y. performed calculations. All contributed to the analysis of the data and writing of the paper.

ADDITIONAL INFORMATION

Supplementary information accompanies the paper on the *npj 2D Materials and Applications* website (https://doi.org/10.1038/s41699-017-0046-y).

Competing interests: The authors declare no competing financial interests.

Publisher's note: Springer Nature remains neutral with regard to jurisdictional claims in published maps and institutional affiliations.

REFERENCES

1. Castro Neto, A. H. et al. The electronic properties of graphene. *Rev. Mod. Phys.* **81**, 109 (2009).
2. Fan, X. B., Zhang, G. L. & Zhang, F. B. Multiple roles of graphene in heterogeneous catalysis. *Chem. Soc. Rev.* **44**, 3023–3035 (2015).
3. Zhou, M., Zhang, A., Dai, Z., Feng, Y. & Zhang, C. Strain-enhanced stabilization and catalytic activity of metal nanoclusters on graphene. *J. Phys. Chem. C.* **114**, 16541–16546 (2010).
4. Zhou, M., Zhang, A., Dai, Z., Zhang, C. & Feng, Y. Greatly enhanced adsorption and catalytic activity of Au and Pt clusters on defective graphene. *J. Chem. Phys.* **132**, 194704–194705 (2010).
5. Lu, Y., Zhou, M., Zhang, C. & Feng, Y. Metal-embedded graphene: a possible catalyst with high activity. *J. Phys. Chem. C.* **113**, 20156–20160 (2009).

6. Zhou, M., Lu, Y., Cai, Y., Zhang, C. & Feng, Y. Adsorption of gas molecules on transition metal embedded graphene: a search for high-performance graphene-based catalysts and gas sensors. *Nanotechnology* **22**, 385502–385509 (2011).
7. Guo, N., Xi, Y., Liu, S. & Zhang, C. Greatly enhancing catalytic activity of graphene by doping the underlying metal substrate. *Sci. Rep.* **5**, 12058 (2015).
8. Wei, Z. J., Hou, Y. X., Yang, Y. & Liu, Y. X. The progress on graphene-based catalysis. *Curr. Org. Chem.* **20**, 2055–2082 (2016).
9. Yang, M., Zhou, M., Zhang, A. & Zhang, C. Graphene oxide: an ideal support for gold nanocatalysts. *J. Phys. Chem. C.* **116**, 22336–22340 (2012).
10. Xiao, F.-X., Miao, J. W. & Liu, B. Layer-by-layer self-assembly of CdS quantum dots/graphene nanosheets hybrid films for photoelectrochemical and photocatalytic applications. *J. Am. Chem. Soc.* **136**, 1559–1569 (2014).
11. Lim, D. et al. Carbon dioxide conversion into hydrocarbon fuels on defective graphene-supported Cu nanoparticles from first principles. *Nanoscale* **6**, 5087–5092 (2014).
12. Marchini, S., Gunther, S. & Wintterlin, J. Scanning tunnelling microscopy of graphene on Ru(0001). *Phys. Rev. B* **76**, 075429 (2007).
13. Sutter, P. W., Flenge, J. I. & Sutter, E. A. Epitaxial graphene on ruthenium. *Nat. Mater.* **7**, 406–411 (2008).
14. Pan, Y. et al. Highly ordered, millimeter-scale, continuous, single-crystalline graphene monolayer formed on Ru (0001). *Adv. Mater.* **21**, 2777–2780 (2009).
15. Feng, W., Lei, S., Li, Q. & Zhao, A. Periodically modulated electronic properties of the epitaxial monolayer graphene on Ru (0001). *J. Phys. Chem. C.* **115**, 24858–24864 (2011).
16. Toyoda, K., Nozawa, K., Matsukawa, N. & Yoshii, S. Density functional theoretical study of graphene on transition-metal surfaces: the role of metal d-band in the potential-energy surface. *J. Phys. Chem. C.* **117**, 8156–8160 (2013).
17. Stradi, D. et al. Lattice-matched versus lattice-mismatched models to describe epitaxial monolayer graphene on Ru(0001). *Phys. Rev. B* **88**, 245401 (2013).
18. Kresse, G. & Hafner, J. *Ab initio* molecular dynamics for liquid metals. *Phys. Rev. B* **47**, 558 (1993).
19. Kresse, G. & Furthmuller, J. Efficient iterative schemes for *ab initio* total-energy calculations using a plane-wave basis set. *Phys. Rev. B* **54**, 11169 (1996).
20. Grimme, S. Semiempirical GGA-type density functional constructed with a long-range dispersion correction. *J. Comp. Chem.* **27**, 1787 (2006).
21. Henkelman, G., Uberuaga, B. & Jónsson, H. A climbing image nudged elastic band method for finding saddle points and minimum energy paths. *J. Chem. Phys.* **113**, 9901–9904 (2000).
22. Perdew, J. P. et al. Atoms, molecules, solids, and surfaces: applications of the generalized gradient approximation for exchange and correlation. *Phys. Rev. B* **46**, 6671–6687 (1992).
23. BlÖchl, P. E. Projector augmented-wave method. *Phys. Rev. B* **50**, 17953–17979 (1994).